

Charge transfer via deep hole in the J51/N2200 blend

Xiaoyu Xie,^{1, a)} Chunfeng Zhang,² and Haibo Ma^{1, b)}

¹⁾*School of Chemistry and Chemical Engineering, Nanjing University, Nanjing 210023, China*

²⁾*National Laboratory of Solid State Microstructures, School of Physics, and Collaborative Innovation Center of Advanced Microstructures, Nanjing University, Nanjing 210093, China.*

(Dated: 13 March 2022)

In recently developed non-fullerene acceptor (NFA) based organic solar cells (OSCs), both the donor and acceptor parts can be excited by absorbing light photons. Therefore, both electron transfer and hole transfer channels could occur at the donor/acceptor interface for generating free charge carriers in NFA based OSCs. However, in many molecular and DNA systems, recent studies revealed the high charge transfer (CT) efficiency cannot be reasonably explained by a CT model with only highest occupied molecular orbitals (HOMOs) and lowest unoccupied molecular orbitals (LUMOs) of donor and acceptor molecules. In this work, taking an example of a full-polymer blend consisting of benzodithiophenealt-benzotriazole copolymers (J51) as donor and naphthalene diimide-bithiophene (N2200) as acceptor, in which the ultrafast hole transfer has been recently reported, we investigate its CT process and examine the different roles of various frontier molecular orbitals. Through a joint study of quantum mechanics electronic structure calculation and nonadiabatic dynamics simulation, we find hole transfer between HOMOs of J51 and N2200 can hardly happen but hole transfer from HOMO of N2200 to HOMO-1 of J51 is much more efficient with a time scale of 3 ps, agreeing well with experiments. This points out the underlying importance of deep hole in CT process and indicates that including frontier molecular orbitals other than HOMO and LUMO is highly necessary to build a robust physical model for studying CT process in molecular optoelectronic materials.

^{a)}Electronic mail: njuxxy2013@gmail.com

^{b)}Electronic mail: haibo@nju.edu.cn

I. INTRODUCTION

Charge transfer (CT) process is one of the key fundamental steps in many molecular optoelectronic materials, ranging from organic solar cells (OSCs)¹⁻¹⁰ to DNA-based nanoelectronics¹¹⁻¹⁴. In organic systems, the interaction between the photo-generated electron-hole pair is very strong with typical binding energy magnitudes of 0.3–1 eV, in large excess of $k_B T$, due to the weakly Coulomb screening with a relative low dielectric permittivity (around 2-3), quite distinct from their inorganic counterparts.¹⁵ Thus, a donor/acceptor (D/A) interface utilizing energy offsets between frontier molecular orbitals (FMOs) in electron donor and acceptor moieties, is usually adopted in these materials to drive an efficient CT before the photoexcitation recombine either radiatively or non-radiatively. Depending on the energetic driving force comes from the photoexcitation in electron donor or acceptor moiety, the CT process is usually classified to electron or hole transfer, i.e. transferring an electron from the lowest unoccupied molecular orbital (LUMO) of donor to the LUMO of acceptor or transferring a hole from the highest occupied molecular orbital (HOMO) of electron acceptor to the HOMO of electron donor. In conventional OSCs electron transfer is considered to dominate the CT at D/A interface^{2,3,16,17}, but hole transfer was recently addressed to be crucial in new OSCs with new non-fullerene acceptor molecules¹⁸⁻²¹, in which the power conversion efficiency (PCE) is boosted to 18.2 %.²¹

Traditionally, energetic and coupling information of only HOMO and LUMO are used in building simplified models for the qualitative or semi-quantitative interpretation of CT processes in molecular systems. In 2014, one of the authors (HM) and Troisi suggested the possibility of additionally utilizing a hot electron via LUMO+1 or a deep hole via HOMO-1 to enhance the CT efficiency by more than two orders of magnitude through reducing the energy barrier for CT, based on an investigation of 5 electron donor molecules and 6 acceptor ones.²² This hypothesis was later supported by a statistical analysis of experimental data from 80 high performing non-fullerene electron acceptors²³, and used in building quantitative structure-property relationship (QSPR) models for predicting PCEs of new OSC molecules²⁴⁻²⁶. In 2015, the generation of hot charge carriers was experimentally verified by terahertz photoconductivity measurements by Lane, et al.¹⁷, in which they found the transfer of an electron following excitation of ZnPc at 400 or 615nm to a higher unoccupied MO of C₆₀. In 2016, Renaud, et al. reported a similar deep hole CT process in DNA hairpins, with an enhancement in CT rates by one hundredfold and much weaker distance dependence.¹⁴ In their work, the authors adopted two different electron acceptors,

stilbenedicarboxamide (SA) and naphthalene-diimide (NDI) at the tail of a DNA hairpin with a same donor stilbenediether (SD) at the head of this DNA hairpin and compared their charge migration performances. Due to the difference in electronic structures of the two acceptors, a much faster and more distance-insensitive CT process has been found in NDI-DNA-SD system via deep hole transfer. All of these studies indicate that, deep occupied MOs (e.g. HOMO-1, HOMO-2 of donor) and high unoccupied MOs (LUMO+1, LUMO+2 of acceptor) other than HOMO and LUMO are also highly necessary to be incorporated in a quantitative CT model and this provides a new promising way to enhance CT efficiency in molecular materials by manipulating their energetics.

Recently, by utilizing ultrafast optical measurements, we found ultrafast hole transfer mediated by intra-moiety polaron pairs²⁷ in the OSC system (PCE: 8.27%)²⁸ consisting of donor benzodithiophenealt-benzotriazole copolymers (J51, whose unit is shown in Fig. 1 (a)) and acceptor naphthalene diimide-bithiophene (N2200, whose unit is shown in Fig. 1 (b)). In this work, we further explore the detailed CT mechanism between J51 and N2200 polymers and investigate the possibility of a deep hole channel by calculating the electronic structure and simulating non-adiabatic dynamics behaviours in J51/N2200 blend. We find that hole transfer between HOMOs of J51 and N2200 can hardly happen but hole transfer from HOMO of N2200 to HOMO-1 of J51 is much more efficient with a ultrafast time scale of 3 ps, agreeing well with our previous experimental measurement. This verifies again the underlying importance of deep hole in CT process and indicates that including frontier molecular orbitals other than HOMO and LUMO is highly necessary to build a robust physical model for studying CT process in molecular optoelectronic materials.

II. METHODOLOGY AND COMPUTATIONAL DETAILS

A. Electron-vibration interaction model

Electron-vibration (el-vib) interaction model is a popular and powerful tool to study exciton/charge processes in molecular aggregated systems. By adopting a linear approximation (truncating high order el-vib interaction), the Hamiltonian for an el-vib coupled system can be expressed as,

$$\hat{H} = \hat{H}_{el} + \hat{H}_{vib} + \hat{H}_{el-vib}, \tag{1}$$

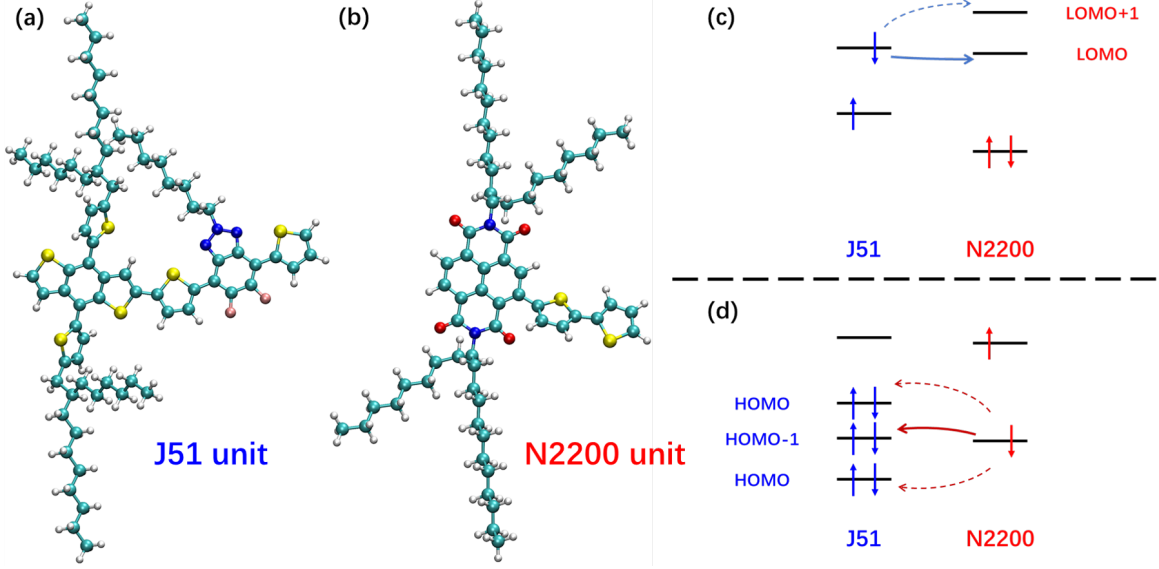


FIG. 1. (a) Unit structure of J51 (donor), (b) unit structure of N2200 (acceptor), (c) schematic electron transfer and (d) schematic hole transfer via deep hole approach for charge transfer process in J51/N2200 blend.

with

$$\hat{H}_{el} = \sum_i \varepsilon_i |\psi_i\rangle \langle \psi_i| + \sum_{i \neq j} V_{ij} |\psi_i\rangle \langle \psi_j|, \quad (2)$$

$$\hat{H}_{vib} = \sum_I \frac{1}{2} \hbar \omega_I \left(-\frac{\partial^2}{\partial Q_I^2} + Q_I^2 \right), \quad (3)$$

$$\hat{H}_{el-vib} = \sum_{i,I} g_i^I Q_I |\psi_i\rangle \langle \psi_i| + \sum_{i,j,I} g_{ij}^I Q_I |\psi_i\rangle \langle \psi_j|. \quad (4)$$

Here, ε_i and V_{ij} represent the energy of the electronic state $|\psi_i\rangle$ and the electronic coupling between $|\psi_i\rangle$ and $|\psi_j\rangle$ under the equilibrium geometry respectively. ω_I is the frequency of the vibration mode I with Q_I being its dimensionless displacement. In the el-vib coupling term, g_i^I are local el-vib couplings and g_{ij}^I are non-local ones.

Considering there are numerous vibration modes in the condensed phase system, spectral density is alternatively used to describe the strength of el-vib couplings with respect to frequency of modes,

$$J_{i/ij}(\omega) = \frac{1}{2\hbar} \sum_I g_{i/ij}^I{}^2 \delta(\omega - \omega_I). \quad (5)$$

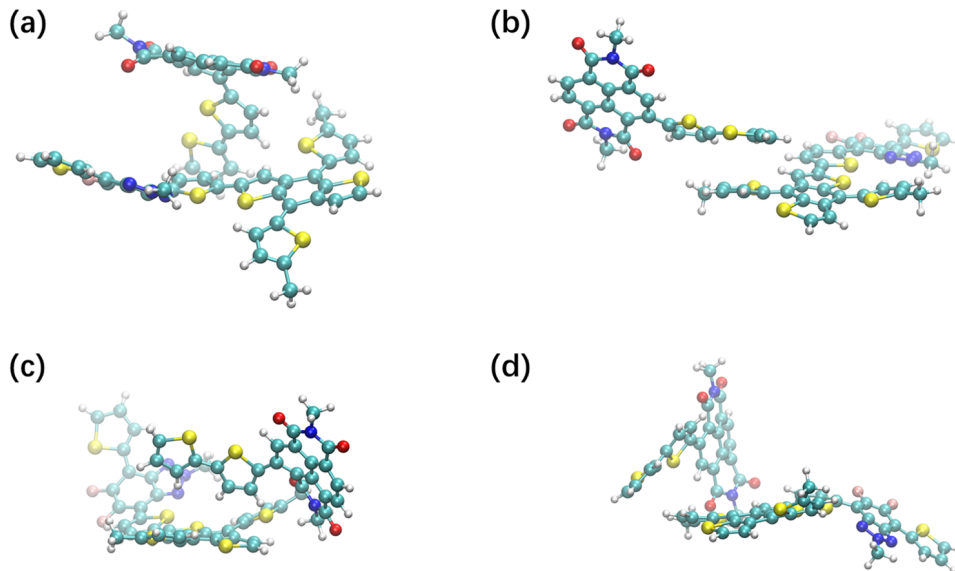


FIG. 2. Selected donor-acceptor pairs for electronic structure calculation (only conjugation skeletons are used): (a) pair 1, (b) pair 2, (c) pair 3 and (d) pair 4.

B. Computational details of parameters in the model

Since the system (polymeric J51/N2200 blend) in our work is amorphous and quite large for *ab initio* calculation, we combine classical molecular dynamics (MD) simulation of an amorphous cell of polymer J51/N2200 blend and quantum mechanical (QM) calculation of neighboring pairs of N2200 and J51 units (see Fig. 2): 1). For ϵ_i and V_{ij} in Eq. 2, we adopt the average values of electronic parameters from sampled MD conformations; 2). Fourier transform of their time auto-correlation function provides information of electron-vibration interaction (i.e. spectral density in Eq. 5).

For the MD part, we build an amorphous cell containing 4 chains of polymer N2200 and J51, with each polymer of J51 and N2200 consisting of 5 units as shown in Fig. 1 (a) and (b) respectively. Then, MD simulation is performed with COMPASSII force field, NPT ensemble (300 K and 1 atm) is used for both geometry relaxation (1 fs per time step until density and temperature of system get nearly equilibrium) and dynamics simulation (10 ps with 1 fs per time step). All MD simulations are done using Materials Studio package²⁹. After the MD simulation, the trajectories of 4 nearest-neighboring pairs of N2200 and J51 unit (alkyl chains are simplified for reducing computational costs) are selected (Fig. 2) for the subsequent electronic structure calculation and further analysis.

For the description of charge transfer at the donor/acceptor interface, we take the one-electron approximation, by considering the weak binding energy of intra-moiety polaron pairs found in this system²⁷, i.e. the electronic states $|\psi_i\rangle$ in Eq. 2 would be reduced to FMOs $|\varphi_i\rangle$. Consequently, parameters in electronic Hamiltonian (Eq. 2) are approximated as the Fock matrix elements of the donor-acceptor system.

$$\varepsilon_i(t) = \pm \langle \varphi_i(t) | \hat{F}(t) | \varphi_i(t) \rangle, \quad (6)$$

$$V_{ij}(t) = \langle \varphi_i(t) | \hat{F}(t) | \varphi_j(t) \rangle, \quad (7)$$

with \hat{F} being the Fock operator of system and t representing the specific conformation of MD trajectory at time t , here sign of $\varepsilon_i(t)$ depends on if it is an occupied MO: '-' for occupied MO (hole transfer) and '+' for unoccupied MO (electronic transfer). Then, we can obtain parameters of electronic Hamiltonian by averaging $\varepsilon_i(t)$ and $V_{ij}(t)$ through the time. In practice, we perform the block-diagonal approach³⁰ to construct localised FMOs and calculate $\varepsilon_i(t)$ and $V_{ij}(t)$. The sampling time interval Δt of conformations is 5 fs with total time $t_{\text{total}} = 10$ ps. i.e. 2000 snapshots are used for each pair in Fig. 2.

Time-dependent value ($\varepsilon_i(t)$ and $V_{ij}(t)$) also contains information of el-vib interaction^{31,32},

$$J_{i/ij}(\omega) = \frac{2}{\pi\hbar} \tanh\left(\frac{\hbar\omega}{2k_{\text{B}}T}\right) \int_0^\infty dt C_{i/ij}(t) \cos(\omega t), \quad (8)$$

here $k_{\text{B}}T$ is the thermal energy with $T = 300$ K in this case and $C_{i/ij}(t)$ is the autocorrelation function of time-dependent $\varepsilon_i(t)/V_{ij}(t)$,

$$C_i(t) = \langle \varepsilon_i(t) \varepsilon_i(0) \rangle - \varepsilon_i^2, \quad (9)$$

$$C_{ij}(t) = \langle V_{ij}(t) V_{ij}(0) \rangle - V_{ij}^2. \quad (10)$$

To reduce the effect of truncated integral problem in Eq. 8, a cosine function $g(t) = \cos(\pi t/t_0)$ with $t_0 = t_{\text{total}}$ is multiplied to autocorrelation function to make the spectral density smooth. In our case, we only consider local spectral density terms for the further dynamics simulation. The non-local terms would be treated in other way, which will be discussed in next Section (Section II C).

C. The Redfield dynamics simulation

As mentioned in Section II A, the degrees of freedom (DoF) of nuclear motion are too large to be treated accurately by a full quantum dynamics theory in a discrete way. A common solution is

using time-dependent equations of reduced density matrix $\rho(t)$ (i.e. quantum master equations) by separating total system into system (\hat{H}_{el}) and bath terms (\hat{H}_{vib}). In our case, we apply the Redfield equation^{31,33–35} in the basis of eigenstates of \hat{H}_{el} ($\hat{H}_{el}|\alpha\rangle = \varepsilon_\alpha|\alpha\rangle$),

$$i\hbar \frac{\partial}{\partial t} \rho_{\alpha\beta}(t) = (\varepsilon_\alpha - \varepsilon_\beta) \rho_{\alpha\beta}(t) - i/\hbar \sum_{\gamma\delta} R_{\alpha\beta\gamma\delta}(t) \rho_{\gamma\delta}(t), \quad (11)$$

where R is the Redfield tensor and given by,

$$R_{\alpha\beta\gamma\delta} = \Gamma_{\delta\beta\alpha\gamma}^+ + \Gamma_{\delta\beta\alpha\gamma}^- - \delta_{\delta\beta} \sum_{\kappa} \Gamma_{\alpha\kappa\kappa\gamma}^+ - \delta_{\alpha\gamma} \sum_{\kappa} \Gamma_{\delta\kappa\kappa\beta}^-, \quad (12)$$

with,

$$\Gamma_{\alpha\beta\gamma\delta}^+(t) = \int_0^t d\tau e^{-i(\varepsilon_\gamma - \varepsilon_\delta)\tau/\hbar} \sum_i C_i^{\text{ther}}(\tau) \langle \alpha | \varphi_i \rangle \langle \varphi_i | \beta \rangle \langle \gamma | \varphi_i \rangle \langle \varphi_i | \delta \rangle, \quad (13)$$

$$\Gamma_{\alpha\beta\gamma\delta}^-(t) = \int_0^t d\tau e^{-i(\varepsilon_\alpha - \varepsilon_\beta)\tau/\hbar} \sum_i C_i^{\text{ther}*}(\tau) \langle \alpha | \varphi_i \rangle \langle \varphi_i | \beta \rangle \langle \gamma | \varphi_i \rangle \langle \varphi_i | \delta \rangle. \quad (14)$$

Here, $C_i^{\text{ther}}(t)$ is the thermal autocorrelation function of ε_i ,

$$C_i^{\text{ther}}(t) = \int_0^\infty d\omega J_i(\omega) \left(\coth \frac{\hbar\omega}{2k_B T} \cos \omega t - i \sin \omega t \right). \quad (15)$$

In practice, the Markovian approximation ($R_{\alpha\beta\gamma\delta}(t) = R_{\alpha\beta\gamma\delta}(+\infty)$) and the secular approximation ($R_{\alpha\beta\gamma\delta} = 0$ for $\varepsilon_\alpha - \varepsilon_\beta \neq \varepsilon_\gamma - \varepsilon_\delta$) are used³⁴.

As shown in Eq. 13, 14 and 15, we only consider the influence of local el-vib couplings. For the non-local terms, we combine the Redfield equation with the frozen-modes (FM) approach³⁶. Since the non-local el-vib couplings are predominated by slow intermolecular modes³⁷, the fluctuation of electronic couplings which caused by nuclear motion can be regarded as static disorders. Thus, the FM approach could be applied to take the non-local el-vib couplings into account. In our work, we replace \hat{H}_{el} by a new \hat{H}'_{el} with,

$$\langle \varphi_i | \hat{H}'_{el} | \varphi_i \rangle = \varepsilon_i, \quad (16)$$

$$\langle \varphi_i | \hat{H}'_{el} | \varphi_j \rangle = V_{ij} + \Delta V_{ij} \text{ with } i \neq j, \quad (17)$$

here ΔV_{ij} is a Gaussian-type random number with standard deviation σ_{ij} which can be obtained from the time-dependent $V_{ij}(t)$. Then, the results of dynamics simulation is computed as statistical average of 1000 trajectory samplings.

TABLE I. Average energies of localised FMOs for four pairs with superscript representing donor (D) or acceptor (A) molecules (Unit: eV)

	HOMO-2 ^D	HOMO-1 ^D	HOMO ^D	HOMO ^A	LUMO ^A	LUMO+1 ^A	LUMO ^D
Pair 1	-7.39	-6.43	-5.76	-6.63	-2.80	-1.85	-2.53
Pair 2	-7.43	-6.51	-5.80	-6.57	-2.88	-1.82	-2.64
Pair 3	-7.44	-6.48	-5.81	-6.44	-2.77	-1.80	-2.74
Pair 4	-7.35	-6.41	-5.72	-6.83	-2.80	-1.86	-2.51

III. RESULTS AND DISCUSSION

A. Electronic structures of MD trajectory snapshots

By using the block diagonal method, we calculate the energies of localised FMOs and electronic couplings between these orbitals for the four neighboring donor-acceptor pairs. The results of orbital energies are shown in Fig. 3, we also list the average values in Tab. I. The energy orders of orbitals for these four pairs are similar and consistent with our schemes in Fig. 1 (c) and (d). For the electron transfer channel, the energies of LUMO+1 of acceptor are significantly higher than LUMO of donor. Therefore, only LUMO-LUMO electron transfer is possible in this system. There are two occupied FMOs of donor whose energies are higher than the energy of HOMO of acceptor or close to it, which implies that there might be more than one path for the hole transfer channel. So, in this work we will focus only on the hole transfer channel in polymeric J51/N2200 blend.

Besides, spatial locations of FMOs of J51 and N2200 units are checked, we find that HOMO and LUMO of N2200 unit locate at bithiophene and naphthalene diimide respectively, which is consistent with the idea of intra-moiety polaron pairs²⁷ and validates our one-electron approximation.

In Fig. 4, we present the electronic coupling results $V(t)$ between HOMO of acceptor and three occupied FMOs of donor. The three couplings in all four pairs behave very similar trajectories (pair 1, pair 2, pair 4 and HOMO-1/HOMO of pair 3) through time, which may result from the similar electronic structures of occupied FMOs of the π -conjugated-structure donor. Unlike the trajectory of energy part in Fig. 3, there are long-wave oscillations for electronic couplings in Fig. 4. These behaviours indicate the interaction between low frequency modes and electronic

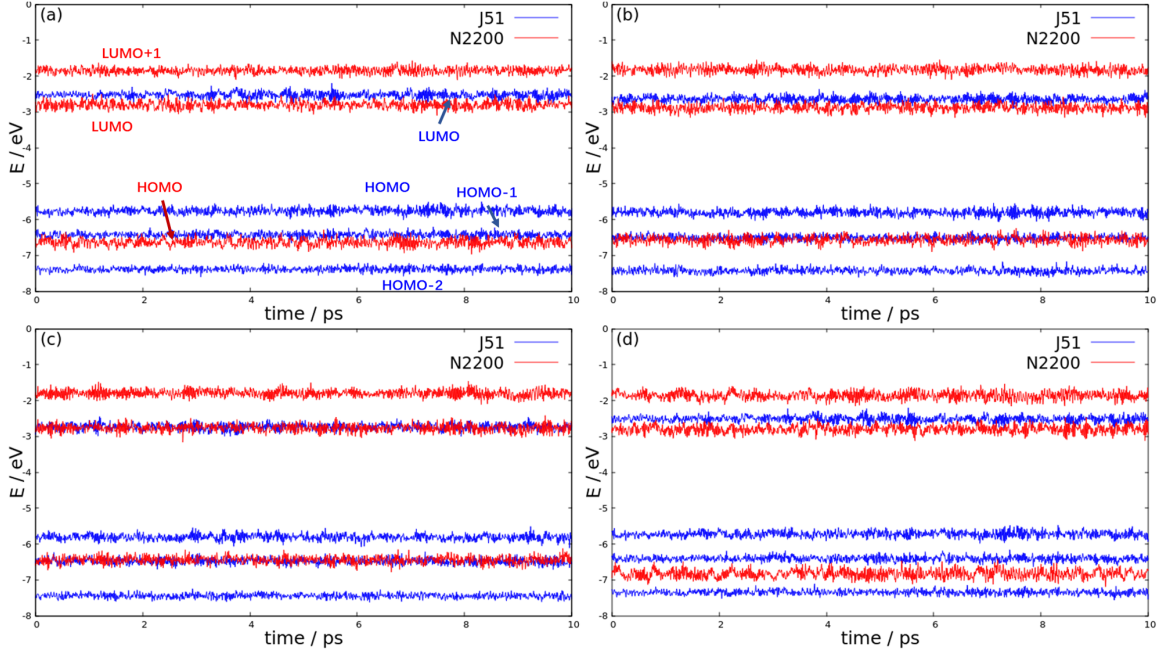


FIG. 3. Energies of localised frontier molecular orbitals (FMOs) of (a) pair 1, (b) pair 2, (c) pair 3 and (d) pair 4. Here blue and red for donor and acceptor respectively.

TABLE II. Average electronic couplings (standard deviation) between HOMO of acceptor and occupied FMOs of donor in four pairs. (Unit: meV)

	HOMO-2 ^D	HOMO-1 ^D	HOMO ^D
Pair 1	11.53 (5.18)	6.09 (5.22)	13.00 (6.91)
Pair 2	8.25 (47.38)	-3.13 (22.41)	8.79 (27.25)
Pair 3	2.25 (8.27)	-14.86 (7.56)	14.02 (7.95)
Pair 4	7.32 (5.44)	6.65 (4.10)	-7.58 (4.68)

couplings, the slow oscillations again validate the FM sampling. The average values and their standard deviations are listed in Tab. II, where the values of these couplings and the standard deviation are around 5-15 meV and 5-10 meV respectively, except the large fluctuations in pair 2.

Both data in Tab. I and II are used to construct electronic Hamiltonian (\hat{H}_{el} in Eq. 2, \hat{H}'_{el} in Eq. 16 and 17) for the dynamics simulations in the next Section (Section III B).

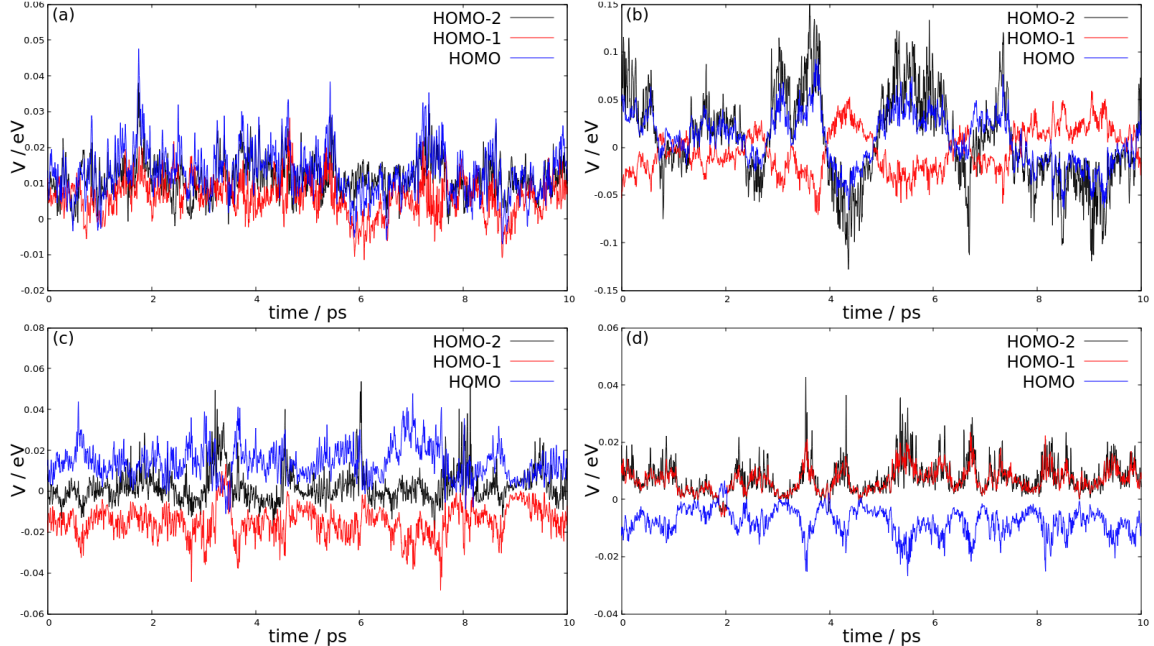


FIG. 4. Electronic couplings between HOMO of acceptor and occupied FMOs of donor for (a) pair 1, (b) pair 2, (c) pair 3 and (d) pair 4.

B. Dynamics results of the Markovian Redfield simulation

To perform the Redfield and Redfield-FM simulation for the hole transfer, information of local el-vib coupling is needed. We compute spectral densities the four orbitals of four pairs via Eq 8. The results are illustrated in Fig. 5, and four pairs show similar peaks for all four orbitals. In this figure, we truncate frequency at 2000 cm^{-1} because the signal is very weak for modes with $\omega > 2000 \text{ cm}^{-1}$, and the reason of the weak signal is that the modes in this region are C-H stretch modes and they do not affect the conjugated skeletons much. Below 2000 cm^{-1} ($\sim 0.25 \text{ eV}$), a general feature of local spectral density is that high frequency modes ($\sim 1700\text{-}1800 \text{ cm}^{-1}$) are dominant. In this region, modes are C-C stretch of the conjugated core and they could change the structure of FMOs and affect their energies. For HOMO of acceptor (N2200 unit), there are non-neglected peaks at around 600 cm^{-1} , the modes in this region can be assigned as breath modes of conjugated core, which affect the structure and energies of FMOs of N2200 unit, too.

With the information in Tab. I, Tab. II (average coupling result) and Fig. 5, the Markovian-approximated Redfield theory is applied to simulate the hole transfer processes for these four pairs, the results in Fig. 6 are different from each other. First, the energy gap between HOMO of acceptor and HOMO/HOMO-2 of donor are larger than the frequency of largest vibration modes (~ 0.25

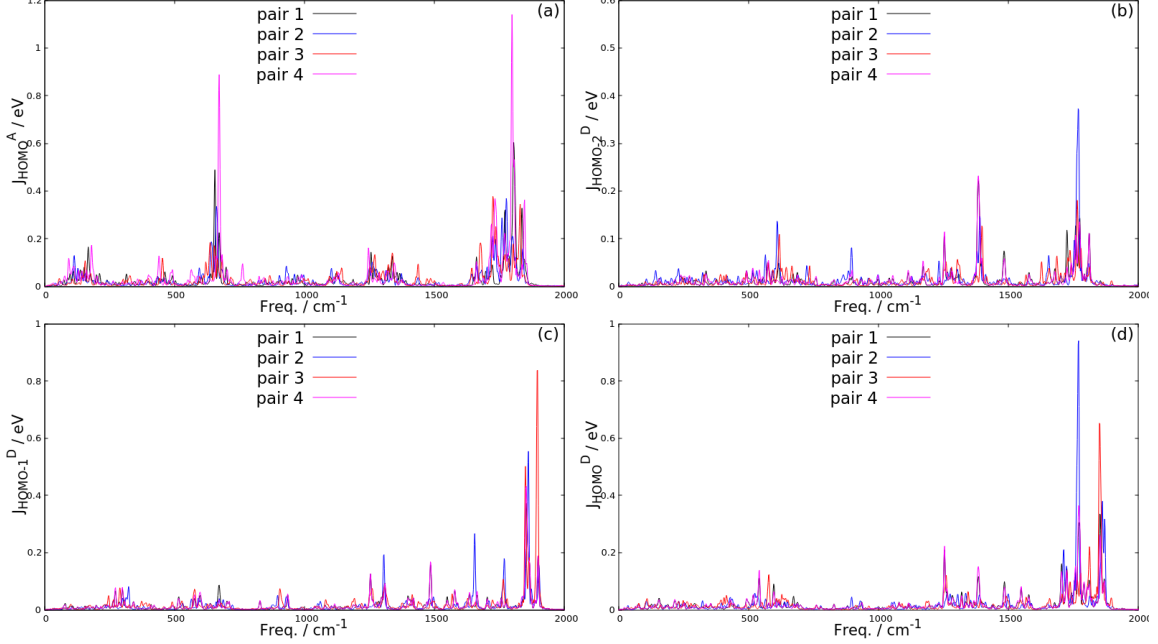


FIG. 5. Spectral densities of local el-vib couplings for (a) HOMO of acceptor, (b) HOMO-2 of donor, (c) HOMO-1 of donor and (d) HOMO of donor.

eV) in Fig. 5. Thus, no population of hole would transfer to these two orbitals. Deep hole transfers via HOMO-1 of donor occur for pair 1, 2 and 3 due to the small energy gap (0.20, 0.06 and -0.04 eV respectively) between HOMO of acceptor and HOMO-1 of donor. With the help of nuclear motion, hole population transfer from HOMO of acceptor to HOMO-1 of donor. In pair 1 and 2, this transfer is exothermal and the hole population at HOMO of acceptor behaves as exponentially decay and the time scale of decay shows good agreement with experimental results of 3 ps²⁷. Besides, the smaller gap and larger electronic coupling in pair 1 lead to a faster transfer. While the endothermal hole transfer in pair 3 converge very fast after the delay oscillation (decoherence). In pair 4, the gap between HOMO-1 of donor and HOMO of acceptor (0.42 eV) is too large to undergo the deep hole transfer, although it is endothermal.

Furthermore, we consider the fluctuation of electronic couplings caused by vibration modes using the Redfield-FM approach. In our work, independent Gaussian disorders are added to three non-zero electronic couplings based on the value of standard deviation (Tab. II), this is contradictory with the fact that the dynamical disorders of these couplings are highly correlated (see Fig. 4 and discussion in Section III A). But in our system, there are typical quasi-two-level-system behaviors shown in Fig. 6 and accordingly our approximation is valid. The time-evolution popula-

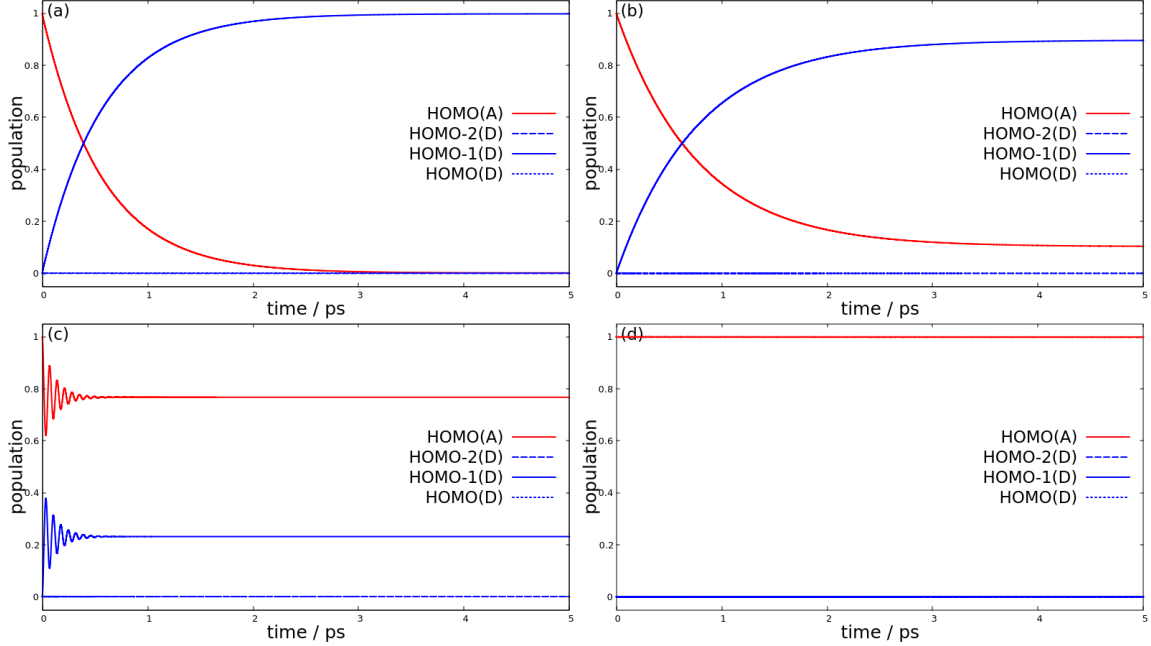


FIG. 6. The Redfield simulation results without FM approach for (a) pair 1, (b) pair 2, (c) pair 3 and (d) pair 4.

tion at HOMO-1 of donor are presented in Fig. 7, comparing to the results of the Redfield equation without FM approach. For exothermal transfer (pair 1 and 2), the final populations at HOMO-1 of donor both decrease, but the changes of rate are different. The rate decreases for pair 1 because σ is comparable to V . Similar effect has been observed for charge mobility of organic semiconductors. i.e. fluctuation of transfer integral slows down mobility of charge³⁸. The increasing rate in pair 2 is owing to the large standard deviation comparing with the average value ($V < \sigma$ and $V \sim 0$). Since the rate k is proportional to $|V|^2$, large fluctuation and near-zero average electronic coupling result to greatly enhanced rate. An extreme limit example can be found in the symmetry breaking singlet fission in rubrene crystal ($V = 0$ with a non-zero σ) recently revealed by ultra-fast spectroscopy experiment³⁹ and theoretical simulation⁴⁰. For the endothermal transfer process (Fig.7 (c)), the fluctuation of electronic coupling is found to be beneficial for the decoherence between two states. But in systems with large energy gap between donor and acceptor orbitals, the fluctuation still can not promote the efficient hole transfer. (see Fig.7 (d))

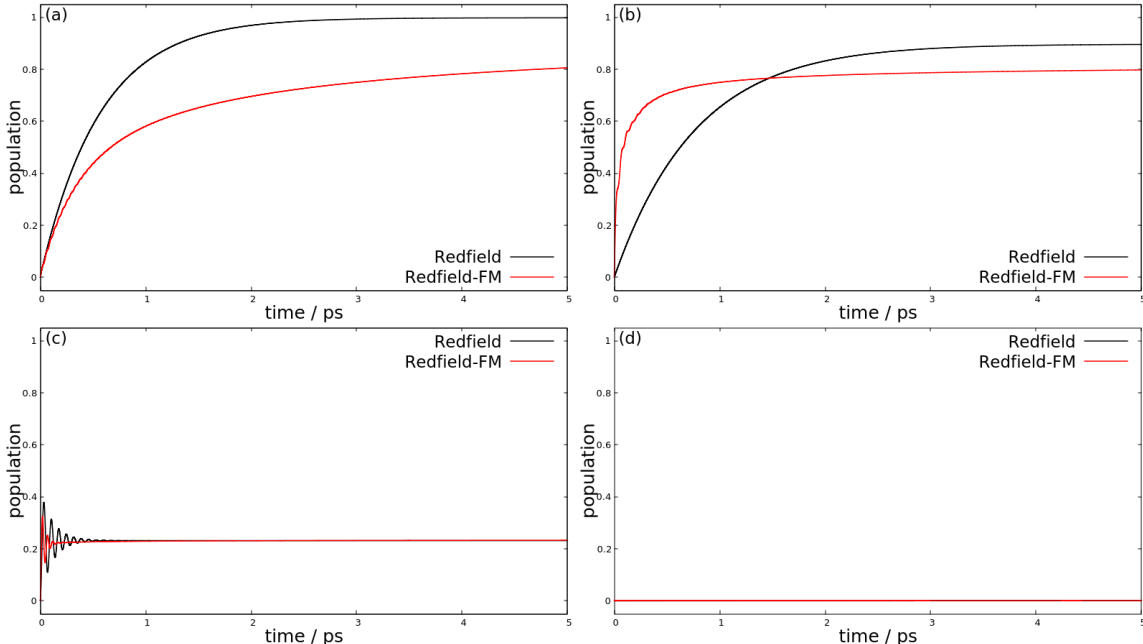


FIG. 7. Comparison of time-evolution hole population at HOMO-1 of donor between the Redfield equation and the Redfield-FM method for (a) pair 1, (b) pair 2, (c) pair 3 and (d) pair 4.

IV. SUMMARY

In this work, we investigate the participation of different FMOs in the ultrafast CT process at J51/N2200 interface. By combining MD simulation of the amorphous blend and QM electronic structure calculation of four selected near-neighboring pairs, we build an el-vib interaction model and simulate nonadiabatic dynamics of hole transfer process of these pairs. Electronic structure calculation shows that energies of HOMO and HOMO-1 of J51 unit are higher than HOMO of N2200, suggesting a high possibility of deep hole transfer in J51/N2200 blend. Time-dependent orbital energies and further spectral density results demonstrate that local el-vib couplings are predominated by high frequency intramolecular modes, while low frequency intermolecular nuclear motions play important roles for non-local el-vib couplings. With the el-vib model, we simulate the hole transfer processes using the Markovian Redfield equation, the results show that deep hole transfer from HOMO-1 of J51 unit to HOMO of N2200 is the only effective path, whose time scale is close to the experimental finding (3 ps). This indicates that, deep occupied MOs (e.g. HOMO-1, HOMO-2 of donor) and high unoccupied MOs (e.g. LUMO+1, LUMO+2 of acceptor) other than HOMO and LUMO are also highly necessary to be incorporated in a quantitative CT model as well. It also provides a new promising way to enhance CT efficiency in molecular materials by

manipulating their energetics.

V. ACKNOWLEDGMENTS

The work was supported by the National Natural Science Foundation of China (Grant No. 21673109).

REFERENCES

- ¹C. Deibel, T. Strobel, and V. Dyakonov, *Adv. Mater.* **22**, 4097 (2010).
- ²T. M. Clarke and J. R. Durrant, *Chem. Rev.* **110**, 6736 (2010).
- ³J. Lee, K. Vandewal, S. R. Yost, M. E. Bahlke, L. Goris, M. A. Baldo, J. V. Manca, and T. Van Voorhis, *J. Am. Chem. Soc.* **132**, 11878 (2010).
- ⁴S. Gélinas, A. Rao, A. Kumar, S. L. Smith, A. W. Chin, J. Clark, T. S. van der Poll, G. C. Bazan, and R. H. Friend, *Science* **343**, 512 (2014).
- ⁵P. Deotare, W. Chang, E. Hontz, D. Congreve, L. Shi, P. Reuswig, B. Modtland, M. Bahlke, C. Lee, A. Willard, *et al.*, *Nat. Mater.* **14**, 1130 (2015).
- ⁶Y. Yao, X. Xie, and H. Ma, *J. Phys. Chem. Lett.* **7**, 4830 (2016).
- ⁷A. W. Kohn, D. P. McMahon, S. Wen, and T. Van Voorhis, *J. Phys. Chem. C* **121**, 26629 (2017).
- ⁸K. M. Pelzer, Á. Vázquez-Mayagoitia, L. E. Ratcliff, S. Tretiak, R. A. Bair, S. K. Gray, T. Van Voorhis, R. E. Larsen, and S. B. Darling, *Chem. Sci.* **8**, 2597 (2017).
- ⁹M. A. Fusella, A. N. Brigeman, M. Welborn, G. E. Purdum, Y. Yan, R. D. Schaller, Y. L. Lin, Y.-L. Loo, T. V. Voorhis, N. C. Giebink, *et al.*, *Adv. Energy Mater.* **8**, 1701494 (2018).
- ¹⁰J. Huang, Y. Mo, and Y. Yao, *Phys. Chem. Chem. Phys.* **21**, 2755 (2019).
- ¹¹J. C. Genereux and J. K. Barton, *Chem. Rev.* **110**, 1642 (2010).
- ¹²K. Kawai and T. Majima, *Acc. Chem. Res.* **46**, 2616 (2013).
- ¹³L. Xiang, J. L. Palma, C. Bruot, V. Mujica, M. A. Ratner, and N. Tao, *Nat. Chem.* **7**, 221 (2015).
- ¹⁴N. Renaud, M. A. Harris, A. P. N. Singh, Y. A. Berlin, M. A. Ratner, M. R. Wasielewski, F. D. Lewis, and F. C. Grozema, *Nat. Chem.* **8**, 1015 (2016).
- ¹⁵M. Bernardi and J. C. Grossman, *Energy Environ. Sci.* **9**, 2197 (2016).
- ¹⁶G. Grancini, M. Maiuri, D. Fazzi, A. Petrozza, H.-J. Egelhaaf, D. Brida, G. Cerullo, and G. Lanzani, *Nat. Mater.* **12**, 29 (2013).

- ¹⁷P. Lane, P. Cunningham, J. Melinger, O. Esenturk, and E. Heilweil, *Nat. Commun.* **6**, 7558 (2015).
- ¹⁸T. Kim, J.-H. Kim, T. E. Kang, C. Lee, H. Kang, M. Shin, C. Wang, B. Ma, U. Jeong, T.-S. Kim, and B. J. Kim, *Nat. Commun.* **6** (2015).
- ¹⁹G. Wang, F. S. Melkonyan, A. Facchetti, and T. J. Marks, *Angew. Chem. Int. Ed.* **58**, 4129 (2019).
- ²⁰C. Lee, S. Lee, G.-U. Kim, W. Lee, and B. J. Kim, *Chem. Rev.* **119**, 8028 (2019).
- ²¹Q. Liu, Y. Jiang, K. Jin, J. Qin, J. Xu, W. Li, J. Xiong, J. Liu, Z. Xiao, K. Sun, S. Yang, X. Zhang, and L. Ding, *Sci. Bull.* **65**, 272 (2020).
- ²²H. Ma and A. Troisi, *J. Phys. Chem. C* **118**, 27272 (2014).
- ²³A. Kuzmich, D. Padula, H. Ma, and A. Troisi, *Energy Environ. Sci.* **10**, 395 (2017).
- ²⁴H. Sahu, W. Rao, A. Troisi, and H. Ma, *Adv. Energy Mater.* **8**, 1801032 (2018).
- ²⁵H. Sahu, F. Yang, X. Ye, J. Ma, W. Fang, and H. Ma, *J. Mater. Chem. A* **7**, 17480 (2019).
- ²⁶H. Sahu and H. Ma, *J. Phys. Chem. Lett.* **10**, 7277 (2019).
- ²⁷R. Wang, Y. Yao, C. Zhang, Y. Zhang, H. Bin, L. Xue, Z.-G. Zhang, X. Xie, H. Ma, X. Wang, Y. Li, and M. Xiao, *Nat. Commun.* **10** (2019).
- ²⁸L. Gao, Z.-G. Zhang, L. Xue, J. Min, J. Zhang, Z. Wei, and Y. Li, *Adv. Mater.* **28**, 1884 (2016).
- ²⁹F. C. Module, Accelrys Inc., San Diego, CA (2013).
- ³⁰Y. Xie, J. Zheng, and Z. Lan, *J. Chem. Phys.* **142**, 084706 (2015).
- ³¹V. May and O. Kühn, *Charge and energy transfer dynamics in molecular systems*, Vol. 2 (Wiley Online Library, 2011).
- ³²M. Aghtar, J. Liebers, J. Strümpfer, K. Schulten, and U. Kleinekathöfer, *J. Chem. Phys.* **136**, 214101 (2012).
- ³³H.-P. Breuer and F. Petruccione, *The theory of open quantum systems* (Oxford University Press on Demand, 2002).
- ³⁴T. C. Berkelbach, M. S. Hybertsen, and D. R. Reichman, *J. Chem. Phys.* **138**, 510 (2013).
- ³⁵R. Tempelaar and D. R. Reichman, *J. Chem. Phys.* **148**, 244701 (2018).
- ³⁶A. Montoya-Castillo, T. C. Berkelbach, and D. R. Reichman, *J. Chem. Phys.* **143**, 194108 (2015).
- ³⁷X. Xie, A. Santana-Bonilla, and A. Troisi, *J. Chem. Theory Comput.* **14**, 3752 (2018).
- ³⁸A. Troisi and G. Orlandi, *Phys. Rev. Lett.* **96**, 086601 (2006).

- ³⁹K. Miyata, Y. Kurashige, K. Watanabe, T. Sugimoto, S. Takahashi, S. Tanaka, J. Takeya, T. Yanai, and Y. Matsumoto, *Nat. Chem.* **9**, 983 (2017).
- ⁴⁰X. Xie, A. Santana-Bonilla, W. Fang, C. Liu, A. Troisi, and H. Ma, *J. Chem. Theory Comput.* **15**, 3721 (2019).